Supporting Information

Predicting flow reversals in chaotic natural convection using data assimilation

By Kameron Decker Harris[1], El Hassan Ridouane[1], Darren L. Hitt[2], and Christopher M. Danforth[1]

[1] *Department of Mathematics and Statistics, Complex Systems Center, & the Vermont Advanced Computing Center, University of Vermont, Burlington, Vermont 05405, USA*

[2] *Department of Mechanical Engineering, University of Vermont, Burlington, Vermont 05405, USA*

(17 April 2012)

APPENDIX S1: Ehrhard-Müller model

S1.1 Derivation

Following the derivations of Gorman et al. (1986) and Ehrhard and Müller (1990), we consider the forces acting upon a control volume of incompressible fluid in the loop. All fluid properties are cross-sectionally averaged, and the radial components of velocity and heat conduction within the fluid are neglected. The fluid velocity $u = u(t)$ is assumed to be constant at all points. Applying Newton's second law, the sum of all forces on the control volume must equal its change in momentum:

$$F_p + F_f + F_g = \rho\pi r^2 R d\phi \frac{du}{dt} \tag{S1-1a}$$

where

$$F_p = -\pi r^2 R\, d\phi \nabla p = -\pi r^2 d\phi \frac{\partial p}{\partial \phi} \tag{S1-1b}$$

$$F_f = -\rho\pi r^2 R\, d\phi\, f_w \tag{S1-1c}$$

$$F_g = -\rho\pi r^2 R\, d\phi\, g \sin\phi\,. \tag{S1-1d}$$

The angular coordinate ϕ and loop dimensions r and R are defined in Fig. 1 in the main text, g is the acceleration of gravity, ρ is the fluid density, u is velocity, and p is pressure. The total force in Eqn. (S1-1a) is comprised of the net pressure (F_p), friction from shear within the fluid (F_f), and the force of gravity (F_g). The pressure term, Eqn. (S1-1b), is the volume times the pressure gradient. The friction term, Eqn. (S1-1c), is written in this form

in order to simplify the analysis; all frictional effects are contained in f_w which will depend on fluid velocity, to be discussed later.

Before we write the momentum equation, it is convenient to apply the Boussinesq approximation, which assumes that variations in fluid density are linear with temperature. In other words, $\rho = \rho(T) \approx \rho_0(1 - \gamma(T - T_0))$ where ρ_0 is the reference density, γ is the coefficient of volumetric thermal expansion, and $T_0 = \frac{1}{2}(T_h + T_c)$ is the reference temperature. The Boussinesq approximation also states that the density variation is insignificant except in terms multiplied by g. Thus, the density ρ is replaced by ρ_0 in all terms of Eqn. (S1-1) except gravity, Eqn. (S1-1d). Using the Boussinesq approximation, gathering terms, and dividing out common factors gives the momentum equation

$$\rho_0 \frac{du}{dt} d\phi = -d\phi \left(\frac{1}{R} \frac{\partial p}{\partial \phi} + \rho_0 \left(1 - \gamma(T - T_0)\right) g \sin\phi + f_w \right) . \tag{S1-2}$$

Integrating about the loop, the momentum equation is simplified because u and f_w are independent of ϕ and other terms drop out due to periodicity.

$$\rho_0 \frac{du}{dt} = \frac{\rho_0 \gamma g}{2\pi} \int_0^{2\pi} d\phi \, T \sin\phi - f_w \tag{S1-3}$$

We now must account for the transfer of energy within the fluid, and between the fluid and the wall. All modes of heat transfer are neglected except convection, which is a valid approximation when $r \ll R$ (Welander, 1967; Ehrhard and Müller, 1990). The energy rate of change (D/Dt is the material derivative with respect to time) in the control volume is

$$\rho_0 \pi r^2 R \, d\phi \, c_p \frac{DT}{Dt} \equiv \rho_0 \pi r^2 R \, d\phi \, c_p \left(\frac{\partial T}{\partial t} + \frac{u}{R} \frac{\partial T}{\partial \phi} \right) \tag{S1-4}$$

which must be equal to the heat transfer through the wall

$$\Delta Q = -\pi r^2 R \, d\phi \, h_w (T - T_w) , \tag{S1-5}$$

where c_p is the specific heat of the fluid, h_w is the heat transfer coefficient, which depends on velocity, and T_w is the temperature at the wall. Combining Eqns. (S1-4) and (S1-5) gives the energy equation

$$\left(\frac{\partial T}{\partial t} + \frac{u}{R} \frac{\partial T}{\partial \phi} \right) = -\frac{h_w}{\rho_0 c_p} (T - T_w) . \tag{S1-6}$$

Together, Eqns. (S1-3) and (S1-6) represent a simple model of the flow in the loop.

The transport coefficients f_w and h_w characterize the interaction between the fluid and the wall. They are defined by the constitutive relations (Ehrhard and Müller, 1990)

$$h_w = h_{w_0} \left[1 + K h(|x_1|)\right] \tag{S1-7}$$

$$f_w = \frac{1}{2} \rho_0 f_{w_0} u , \tag{S1-8}$$

where $x_1 \propto u$ is the dimensionless velocity. The function

$$h(x) = \begin{cases} p(x) & \text{when } x < 1 \\ x^{1/3} & \text{when } x \geqslant 1 \end{cases} \tag{S1-9}$$

in Eqn. (S1-7) determines the velocity dependence of the heat transfer coefficient, which varies as $u^{1/3}$ for moderate u (Ehrhard and Müller, 1990). We introduce the fitting polynomial $p(x) = 44/9\,x^2 - 55/9\,x^3 + 20/9\,x^4$ to ensure that h_w is analytic at $x_1 = 0$. This piecewise definition causes $h(x)$ to vary as $p(x)$ for $x \leqslant 1$ and $x^{1/3}$ for $x > 1$. Eqn. (S1-8) gives the frictional deceleration of the fluid when $|u| > 0$, and the $\rho_0/2$ term is retained to simplify the final solution. Dimensionally, f_w is an acceleration ($\mathrm{m/s^2}$) and h_w is power per unit volume per unit temperature ($\mathrm{W/m^3K}$). These coefficients h_{w_0}, f_{w_0}, and K must be estimated from experiments (e.g., Ehrhard and Müller, 1990; Welander, 1967; Gorman et al., 1986) or from other empirical means. In Sec. S1.2, we describe the empirical methods used for parameter estimation.

Ehrhard and Müller (1990) solved the system of two coupled, partial differential equations (Eqns. (S1-3) and (S1-6)) by introducing an infinite Fourier series for T. The essential dynamics can be captured by the lowest modes, i.e.,

$$T(\phi, t) = C_0(t) + S(t)\sin\phi + C(t)\cos\phi\,. \tag{S1-10}$$

Because this form of T separates the variables ϕ and t, the problem is transformed into a set of ordinary differential equations. Substituting Eqn. (S1-10) into Eqn. (S1-3) and integrating gives the equation of motion for u. Similarly, Eqn. (S1-6) is integrated by $\oint d\phi \sin\phi$ and $\oint d\phi \cos\phi$ to separate the two temperature modes S and C. The system is written in dimensionless form

$$\frac{dx_1}{dt'} = \alpha\,(x_2 - x_1) \tag{S1-11a}$$

$$\frac{dx_2}{dt'} = \beta x_1 - x_2\,(1 + Kh(|x_1|)) - x_1 x_3 \tag{S1-11b}$$

$$\frac{dx_3}{dt'} = x_1 x_2 - x_3\,(1 + Kh(|x_1|)) \tag{S1-11c}$$

where the following linear transformations have been made to create dimensionless variables

$$\left.\begin{aligned} t' &= \frac{h_{w_0}}{\rho_0 c_p} t \\ x_1 &= \frac{\rho_0 c_p}{R h_{w_0}} u \\ x_2 &= \frac{1}{2} \frac{\rho_0 c_p \gamma g}{R h_{w_0} f_{w_0}} \Delta T_{3-9} \\ x_3 &= \frac{1}{2} \frac{\rho_0 c_p \gamma g}{R h_{w_0} f_{w_0}} \left(\frac{4}{\pi} \Delta T_w - \Delta T_{6-12} \right) . \end{aligned}\right\} \tag{S1-12}$$

Physically, x_1 is proportional to the mean fluid velocity, x_2 to the temperature difference across the convection cell or ΔT_{3-9} (between 3 o'clock and 9 o'clock), and x_3 is proportional to the deviation of the vertical temperature profile (characterized by the temperature difference between 6 o'clock and 12 o'clock, ΔT_{6-12}) from the value it takes during conduction.

The parameter $\alpha = \frac{1}{2}\rho_0 c_p f_{w_0}/h_{w_0}$ is comparable to the Prandtl number, the ratio of momentum diffusivity and thermal diffusivity. Similar to the Rayleigh number, the heating parameter

$$\beta = \frac{2}{\pi} \frac{\rho_0 c_p \gamma g}{R h_{w_0} f_{w_0}} \Delta T_w \tag{S1-13}$$

determines the onset of convection as well as the transition to chaotic behavior.

Although the previous derivation assumes a 3D geometry, the CFD simulations described in Sec. 2.1 of the main text, were performed in 2D. A 2D geometry corresponds to infinite concentric cylinders as opposed to the quasi-1D torus. Due to cross-sectional averaging, the EM equations of motion (S1-11) are the same in 2D or 3D; the change may be realized by letting $\pi r^2 \to 2r$ in Eqns. (S1-1), (S1-4), and (S1-5) and carrying out the rest of the derivation. The only differences arise in the non-dimensional transformations and parameters, which were empirically determined by a multiple shooting algorithm (see Sec. S1.2).

S1.2 Parameter estimation

Before any forecasting, the parameters matching the EM model to the thermosyphon simulation needed to be determined. Ehrhard and Müller (1990) used experimental measurements to determine the correlation coefficients for friction, f_{w_0}, and heat transfer, h_{w_0} and K. They achieved this by opening the loop at $\phi = \pi/2$ and providing a developed flow with adjustable velocity. By measuring the pressure loss ($\propto f_w$) and heat transfer across the loop for a range of velocities, they were able to find the correlation coefficients using regression. We were unable to accomplish this with a CFD simulation of an open-loop geometry.

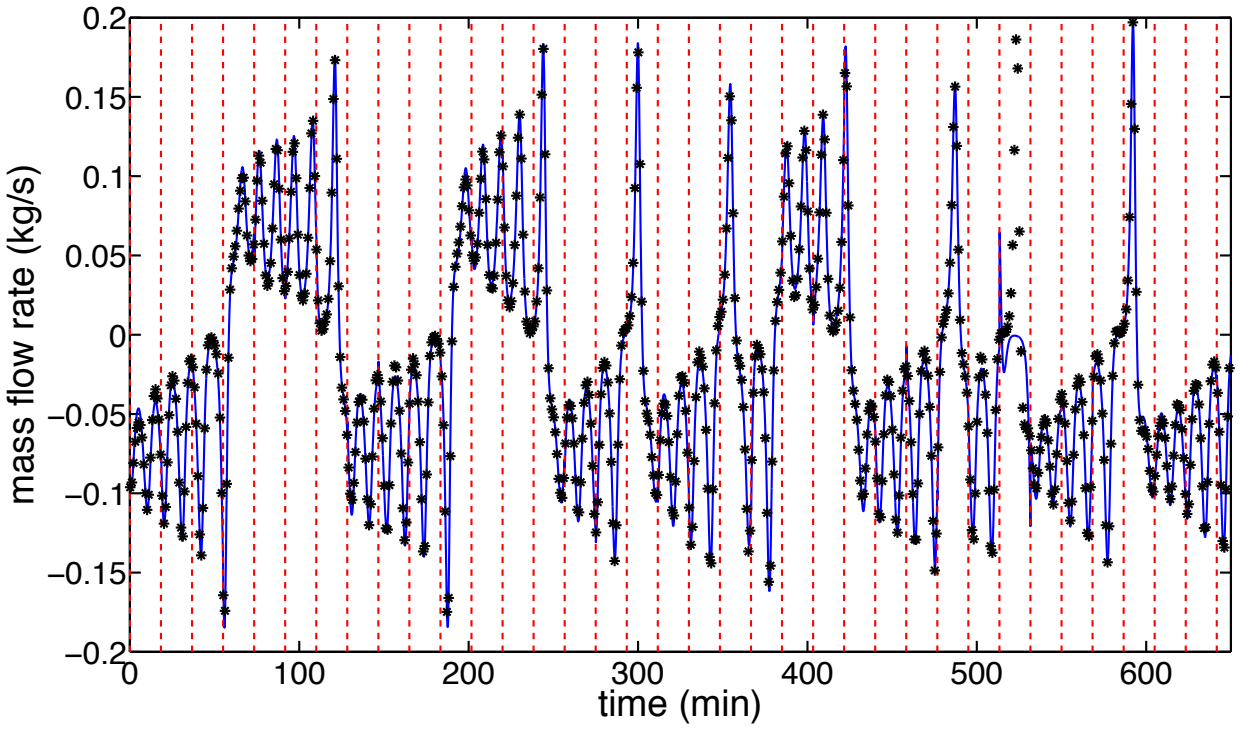

Figure S1-1. Results of the multiple shooting algorithm. The entire training timeseries is shown. Starred points are the CFD thermosyphon mass flow rate data used for validation. Also shown are the trajectories of model integrations over each shooting window, which are indicated by the dashed vertical lines. In one shooting window, near 515 min, the model does not match the data because the optimization has not found a good IC (it is near the highly unstable conducting equilibrium) even though the parameters are acceptable.

parameter	value
α	7.99
β	27.3
K	0.148
t scale (s)	631.6
q scale (kg/s)	0.0136

Table S1-1. Final parameters used in the data assimilation scheme. The first three are the dimensionless parameters of the model, and the final two are used to rescale the dimensionless time and mass flow rate.

Instead, parameter estimation was formulated as a multiple shooting problem. Shooting methods minimize the error in an ODE trajectory relative to data by optimizing over all possible initial conditions and parameter space. Multiple shooting is a shooting method suitable for chaotic ODEs (Baake et al., 1992). It overcomes the sensitive dependence on initial conditions by partitioning the data set and solving the shooting problem on those subsets of the data, augmented by continuity conditions. We used the nonlinear least square optimizer `lsqnonlin` in Matlab (2009) to perform the minimization and relaxed the continuity constraints. The model parameters which were tuned were α, β, and K. However, we also needed a way to determine the time and velocity scales to convert the dimensionless variables t' and x_1 to their observed, dimensional values t and q. These scales change as the other parameters are varied, so these were incorporated into the variables of the optimization.

The results of the multiple shooting algorithm are shown in Fig. S1-1 and Table S1-1.

APPENDIX S2: Data assimilation algorithms

S2.1 Kalman Filter (KF)

The KF is well-known and widely used in linear DA and control problems. Although the thermosyphon is highly nonlinear, the linear update equations are similar to those of the nonlinear algorithms used for this experiment. The KF attempts to assimilate observations and forecasts for a process of the form

$$\mathbf{x}_k^t = \mathbf{W}\mathbf{x}_{k-1}^t \,. \tag{S2-1}$$

In this case, $\mathbf{x}^t$ is the true state, which advances in time according to the linear process $\mathbf{W}$, which is unknown but approximated by the model $\mathbf{M}$. Subscripts index the time step. Using the model, the analysis from the previous time step is integrated to generate the background forecast for the current time step

$$\mathbf{x}_k^b = \mathbf{M}\mathbf{x}_{k-1}^a \tag{S2-2}$$

where $\mathbf{M}$ is the linear model, $\mathbf{x}^a$ is the old analysis, and $\mathbf{x}^b$ is the background. Because $\mathbf{M}$ is only an approximation of $\mathbf{W}$, a perfect initial condition will not lead to a perfect forecast, so

$$\mathbf{x}_k^t = \mathbf{M}\mathbf{x}_{k-1}^t + \epsilon_k^q \tag{S2-3}$$

where the model errors ϵ^q have covariance $\mathbf{Q}$ (usually assumed to be constant in time) and are written on the right hand side for convenience. When deemed unnecessary, time subscripts are left out.

Given an observation $\mathbf{y}$ and background forecast $\mathbf{x}^b$, the KF finds the optimal way to combine them into the *analysis* $\mathbf{x}^a$, the best guess of the current state. This becomes the IC when forecasting with the model, Eqn. (S2-2). In an operational context, we usually cannot observe every state variable. If $\mathbf{x} \in \mathbb{R}^N$ and $\mathbf{y} \in \mathbb{R}^M$, then $M < N$ (in NWP $M \ll N$), so we define the observation operator $\mathcal{H} : \mathbb{R}^N \to \mathbb{R}^M$ that takes the background forecast from the model state space into the observation space. This serves two purposes: first, it avoids extrapolation of observations to gridpoints in state space; and second, it enables us to interpret our forecasts by comparing them directly to observations. For the thermosyphon, $\mathcal{H}$ is linear, so we write it as $\mathbf{H}$, but this is usually not the case for the observations in NWP, e.g., satellite radiances and radar reflectivities.

The complete application of the KF consists of a forecast step

$$\mathbf{x}_k^b = \mathbf{M}\mathbf{x}_{k-1}^a \tag{S2-4a}$$

$$\mathbf{B}_k = \mathbf{M}\mathbf{A}_{k-1}\mathbf{M}^T + \mathbf{Q} \tag{S2-4b}$$

and an analysis step

$$\mathbf{x}_k^a = \mathbf{x}_k^b + \mathbf{K}_k(\mathbf{y}_k - \mathbf{H}\mathbf{x}_k^b) \tag{S2-5a}$$

$$\mathbf{A}_k = (1 - \mathbf{K}_k\mathbf{H})\mathbf{B}_k \tag{S2-5b}$$

with the Kalman gain $\mathbf{K}_k$ given by

$$\mathbf{K}_k = \mathbf{B}_k\mathbf{H}^T(\mathbf{H}\mathbf{B}_k\mathbf{H}^T + \mathbf{R})^{-1}\,. \tag{S2-6}$$

The forecast equations create the background forecast and update the background error covariance. The new background error covariance is the old analysis error integrated forward plus the model error $\mathbf{Q}$. In the analysis step, this background forecast is incremented by the gain times the innovation $(\mathbf{y} - \mathbf{H}\mathbf{x}^b)$ to produce the analysis. The difference between the analysis and the background is referred to as the *analysis increment*; statistical properties of these increments can be used to reduce model error (Danforth et al., 2007; Danforth and Kalnay, 2008b;a). The new analysis error is equal to the background error reduced by a factor of $(1 - \mathbf{KH})$. By finding the analysis, the filter has revealed the best possible starting point for the next background forecast. In fact, if the system is linear, the KF is the optimal algorithm for state-estimation.

S2.2 Variational Filtering (3D-Var)

Rather than minimize the analysis error variance, the analysis equations can also be derived by finding the analysis state $\mathbf{x}^a$ that minimizes the quadratic scalar cost function $2C(\mathbf{x}) = (\mathbf{x} - \mathbf{x}^b)^T\mathbf{B}^{-1}(\mathbf{x} - \mathbf{x}^b) + (\mathbf{y} - \mathcal{H}\mathbf{x})^T\mathbf{R}^{-1}(\mathbf{y} - \mathcal{H}\mathbf{x})$. The cost $C(\mathbf{x})$ has its minimum at $\mathbf{x} = \mathbf{x}^a$, where $\mathbf{x}^a$ is given by Eqn. (S2-5). This is called the 3D variational (3D-Var) method since the minimization for NWP is with respect to a state vector embedded in a three-dimensional field (latitude, longitude, and height).

Formally, both 3D-Var and the KF yield the same solution (Kalnay, 2002). However, in this case the control variable is the analysis, while in the KF the control variable is the weight matrix itself. In operational NWP, where the dimension of the state space N is of $\mathcal{O}(10^9)$, the numerical implementations of 3D-Var and the nonlinear KF are drastically different. Because 3D-Var assumes the background error $\mathbf{B}$ is fixed in time, the Kalman gain $\mathbf{K}$ needs

to be calculated only once. The calculation of $\mathbf{K}$ is the most computationally prohibitive part of DA because it requires solving a linear system in N variables. A constant $\mathbf{K}$ thus makes the algorithm computationally simple; the most difficult part of implementing 3D-Var is finding the optimal $\mathbf{B}$.

However, a static $\mathbf{B}$ is not realistic. From a dynamical systems standpoint, uncertainty is closely related to stability, which is clearly dependent on the system state. In the thermosyphon, the true background error is typically smaller when the system state is near the unstable convecting equilibria than when the state is near the more unstable conducting equilibrium. Because 3D-Var is computationally cheap, the National Centers for Environmental Prediction (NCEP) employ it to estimate ICs for the National Weather Service 14-day global forecasts. However, it cannot detect so-called "errors of the day", state-dependent forecast errors which grow quickly but are not represented in the 3D-Var background error covariance matrix (Kalnay, 2002; Li et al., 2009).

In our implementation, the 3D-Var background error covariance $\mathbf{B}_{\text{3D-Var}}$ was calculated iteratively, using a techniques similar to that described in Yang et al. (2006). We did this by calculating a time average of the outer product of analysis increments

$$\mathbf{B}_{\text{3D-Var}} = \langle (\mathbf{x}^b - \mathbf{x}^a)(\mathbf{x}^b - \mathbf{x}^a)^T \rangle, \tag{S2-7}$$

disregarding the initial 500 assimilation cycles and iterating the process until convergence. During this, forecast errors were observed to decrease and stabilize. This $\mathbf{B}_{\text{3D-Var}}$ was first computed for the 30 s assimilation window. It was stored and then used to bootstrap the iterative procedure for the 60 s assimilation window, which was stored and fed into the calculation for the 90 s assimilation window, etc.

S2.3 Extended Kalman Filter (EKF)

The EKF is essentially the KF applied to a nonlinear model. Given a nonlinear model $\mathcal{M}$, the error covariances are updated by the *linear tangent model* $\mathbf{M} \equiv \partial\mathcal{M}/\partial\mathbf{x}|_{\mathbf{x}=\mathbf{x}^b}$ which takes the place of $\mathbf{M}$ in Eqn. (S2-4b). This model propagates small perturbations around the trajectory $\mathbf{x}^b$ forward in time. To operate on the matrix $\mathbf{A}$ with the linear tangent model, first take the Jacobian of F (the right hand side of the nonlinear differential equation $\dot{\mathbf{x}} = F(\mathbf{x})$ which describes the model $\mathcal{M}$) and evaluate it at the background point $\mathbf{x}^b$; call this matrix $\mathbf{J}$. Each column $\mathbf{a}_i$ of $\mathbf{A}$, which can be thought of as an error perturbation to the analysis state, is then integrated forward in time according to the linear ODE $\dot{\mathbf{a}}_i = \mathbf{J}\,\mathbf{a}_i$.

Also note that if the observation operator $\mathcal{H}$ is nonlinear, it is replaced by a similar linear tangent model $\mathbf{H}$ in the matrix equations (S2-5) and (S2-6). The transpose of these matrix functions are called *adjoint models*, which are used in sensitivity analysis of the state to perturbations.

To propagate the background covariance without the explicit adjoint model, as Eqn. (S2-4b) would require, $\mathbf{B}$ was first decomposed with the Cholesky factorization (Golub and van Loan, 1996) into the product of a lower and upper diagonal matrix before its columns were integrated forward with the linear tangent model $\mathbf{M}$.

$$\mathbf{B}_{k-1} = \mathbf{L}_{k-1}\mathbf{L}_{k-1}^T \tag{S2-8}$$

$$\mathbf{T}_k = \mathbf{M}_{k-1}\mathbf{L}_{k-1} \tag{S2-9}$$

$$\mathbf{A}_k = \mathbf{T}_k\mathbf{T}_k^T + \mathbf{Q} \tag{S2-10}$$

This guarantees symmetry for the new analysis error covariance $\mathbf{A}$.

Some modifications to the EKF algorithm are necessary to prevent filter divergence. A multiplicative inflation factor

$$\mathbf{B} \leftarrow (1 + \Delta)\mathbf{B} \tag{S2-11}$$

was applied to the background covariance matrix after the model integration and before the analysis step. We also performed additive inflation, following Yang et al. (2006). Random numbers uniformly distributed between 0 and μ were added to the diagonal elements of $\mathbf{A}$ after performing the analysis and before the next forecast step, i.e.

$$\mathbf{A} \leftarrow \mathbf{A} + \mu \, \mathrm{diag}(\nu) \tag{S2-12}$$

where ν is an N-dimensional vector whose entries are drawn from a uniform distribution between 0 and 1.

S2.4 Ensemble Kalman Filters (EnKFs)

The EnKF is a method that replaces a single forecast state with an ensemble of states. The spread of the ensemble about its mean gives an approximation of the background error covariance and forecast uncertainty, while the ensemble average gives the best guess of the forecast. The EnKF was first introduced by Evensen (1994). For a comprehensive overview of ensemble filters, see Evensen (2003). It was shown that if the observation, which has random error with covariance $\mathbf{R}$, is perturbed with P random errors (again with covariance $\mathbf{R}$), to make an P-member ensemble of independent observations $\{\mathbf{y}_i\}$, then the background

error covariance can be written (Evensen, 2003)

$$\mathbf{B} \approx \frac{1}{P-1}\sum_{i=1}^{P}(\mathbf{x}_i^b - \overline{\mathbf{x}^b})(\mathbf{x}_i^b - \overline{\mathbf{x}^b})^T = \frac{1}{P-1}\mathbf{X}^b\mathbf{X}^{bT} \tag{S2-13}$$

which is simply the unbiased average outer product of background perturbations $\mathbf{X}^b = [\mathbf{x}_1'^b, \ldots, \mathbf{x}_P'^b]$. The background forecast of ensemble member i is denoted $\mathbf{x}_i^b$, $\overline{\mathbf{x}^b}$ is the background forecast ensemble average, and $\mathbf{x}_i'^b = \mathbf{x}_i^b - \overline{\mathbf{x}^b}$ is the ith member's deviation from the mean. In this case, each ensemble member is updated according to the KF equations for their associated observation

The advantages of the EnKF are many: there is no linear tangent model to compute, the number of ensemble members can be small ($\mathcal{O}(10^2)$ for NWP) relative to the dimensionality of the state space, and prior knowledge about the structure of the forecast errors is not necessary. Currently, 4D-Var (like 3D-Var but also taking into account older observations) and ensemble filters are the most promising candidates being considered to replace 3D-Var in operational NWP.

As with the EKF, ensemble filters tend to underestimate the background error, resulting in an ensemble spread which is typically less too small. We again used multiplicative inflation of the background error, a common method shown to be successful in Evensen (2003); Whitaker and Hamill (2002); Annan and Hargreaves (2004); Yang et al. (2006); Kalnay et al. (2007). This is accomplished by setting

$$\mathbf{X}^b \leftarrow (1+\Delta)^{1/2}\mathbf{X}^b \tag{S2-14}$$

before the analysis step. Additive inflation proved crucial to stabilizing both EnKFs tested. Without it, the filters sometimes worked but only with $\Delta \gg 1$; Δ is supposed to be a small parameter. As in the EKF, additive inflation is applied immediately after the analysis step, but in this case the noise is added to the analysis ensemble states

$$\mathbf{x}_i^a \leftarrow \mathbf{x}_i^a + \mu\,\nu \tag{S2-15}$$

for all $i = 1, \ldots, P$. The noise ν is, again, an N-dimensional random vector with entries drawn from the uniform distribution between 0 and 1.

S2.5 Ensemble Square Root Filter (EnSRF)

The original EnKF adds noise to create linearly independent observations and is classified as a *perturbed observations* method (Kalnay et al., 2007). This necessarily introduces additional sampling error into the forecast. For this reason, Whitaker and Hamill (2002)

introduced the ensemble square root filter (EnSRF) as an improved EnKF. In the EnSRF, the ensemble mean is updated with the traditional Kalman gain (Eqn. (S2-6))

$$\overline{\mathbf{x}^a} = \overline{\mathbf{x}^b} + \mathbf{K}(\mathbf{y} - \mathcal{H}\overline{\mathbf{x}^b}) \tag{S2-16}$$

and deviations from the mean are updated by

$$\mathbf{X}^a = (1 - \tilde{\mathbf{K}}\mathcal{H})\mathbf{X}^b \tag{S2-17}$$

where

$$\tilde{\mathbf{K}} = \mathbf{B}\mathbf{H}^T \left[\left(\sqrt{\mathbf{H}\mathbf{B}\mathbf{H}^T + \mathbf{R}} \right)^{-1} \right]^T \times \left[\sqrt{\mathbf{H}\mathbf{B}\mathbf{H}^T + \mathbf{R}} + \sqrt{\mathbf{R}} \right]^{-1} . \tag{S2-18}$$

When the observation is a scalar, it can be shown that

$$\tilde{\mathbf{K}} = \left(1 + \sqrt{\frac{\mathbf{R}}{\mathbf{H}\mathbf{B}\mathbf{H}^T + \mathbf{R}}} \right)^{-1} \mathbf{K} . \tag{S2-19}$$

If observation errors are uncorrelated ($\mathbf{R}$ is diagonal), then Eqn. (S2-19) can be used to process observations one at a time (Whitaker and Hamill, 2002). The updated analysis ensemble is then $\{\mathbf{x}_i^a\}$, where $\mathbf{x}_i^a = \overline{\mathbf{x}^a} + \mathbf{x}_i'^a$. Square root filters have better numerical stability and speed than their standard KF counterparts. The Potter square root filter was employed for navigation in the Lunar Module of the Apollo program (Savely et al., 1972).

S2.6 Ensemble Transform Kalman Filter (ETKF)

The ETKF is another type of deterministic square root filter. In this variant, the analysis perturbations are assumed to be equal to the background perturbations postmultiplied by a transformation matrix $\mathbf{T}$ so that the analysis error covariance satisfies Eqn. (S2-5b). The analysis covariance is written

$$\mathbf{A} = \frac{1}{P-1}\mathbf{X}^a\mathbf{X}^{aT} = \mathbf{X}^b\hat{\mathbf{A}}\mathbf{X}^{bT}$$

where $\hat{\mathbf{A}} = [(P-1)\mathbf{I} + (\mathbf{H}\mathbf{X}^b)^T\mathbf{R}^{-1}(\mathbf{H}\mathbf{X}^b)]^{-1}$. The analysis perturbations are $\mathbf{X}^a = \mathbf{X}^b\mathbf{T}$, where $\mathbf{T} = [(P-1)\hat{\mathbf{A}}]^{1/2}$. See Kalnay et al. (2007) for further details.

The local ensemble transform filter (LETKF) is a variant that computes the analysis at a given gridpoint using only local observations. This allows for efficient parallelization. Localization removes spurious long-distance correlations from $\mathbf{B}$ and allows greater flexibility in the global analysis by allowing different linear combinations of ensemble members at different spatial locations (Kalnay et al., 2007; Hunt et al., 2007).

EnSRF & ETKF			EKF		
analysis window (s)	Δ	μ	analysis window (s)	Δ	μ
30	0.15	0.25	30	0.15	0.25
60	0.15	0.25	60	0.15	0.25
90	0.15	0.25	90	0.15	0.25
120	0.15	0.25	120	0.15	0.25
150	0.15	0.25	150	0.15	0.25
180	0.15	0.25	180	0.15	0.25
210	0.15	0.25	210	0.15	0.25
240	0.15	0.25	240	0.15	0.25
270	0.15	0.25	270	0.15	0.25
300	0.15	0.25	300	0.15	0.25
330	0.15	0.25	330	0.15	0.25
360	0.15	0.25	360	0.15	0.25
390	0.2	0.25	390	0.2	0.25
420	0.2	0.25	420	0.2	0.25
450	0.2	0.25	450	0.2	0.25
480	0.25	0.25	480	0.2	0.25
510	0.25	0.25	510	0.2	0.25
540	0.25	0.25	540	0.25	0.25
570	0.25	0.25	570	0.25	0.25
600	0.25	0.25	600	0.25	0.25

Table S2-1. Inflation tuning parameters used in DA experiments.

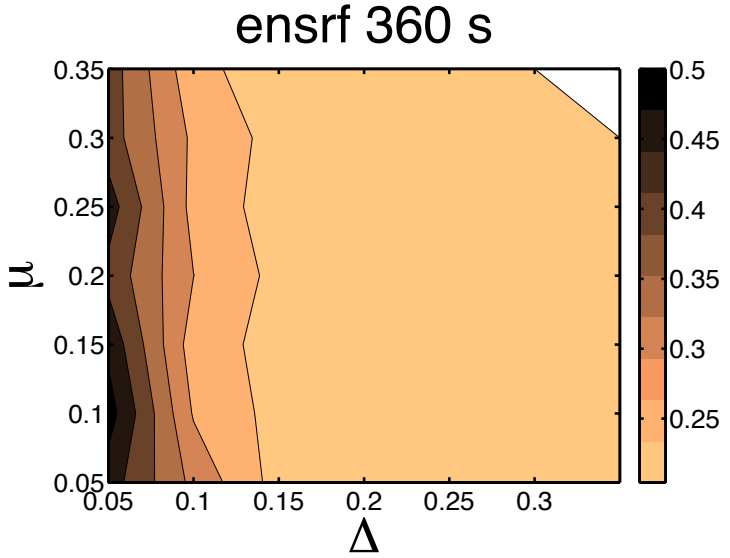

Figure S2-1. Contour plot of forecast error using the EnSRF and an assimilation window of 360 s, as the inflation parameters Δ and μ were varied. The chosen parameters $\Delta = 0.15$ and $\mu = 0.25$ lie in the region of lowest error.

S2.7 Tuning Parameters

Table S2-1 lists the tuning parameters used for the DA experiments. The tuning was done manually. Sensitivity of model error to the tuning parameters was checked by creating a course contour plot of background error for assimilation windows of 2, 4, 6, 8, and 10 minutes for each filter; an example is shown in Fig. S2-1.

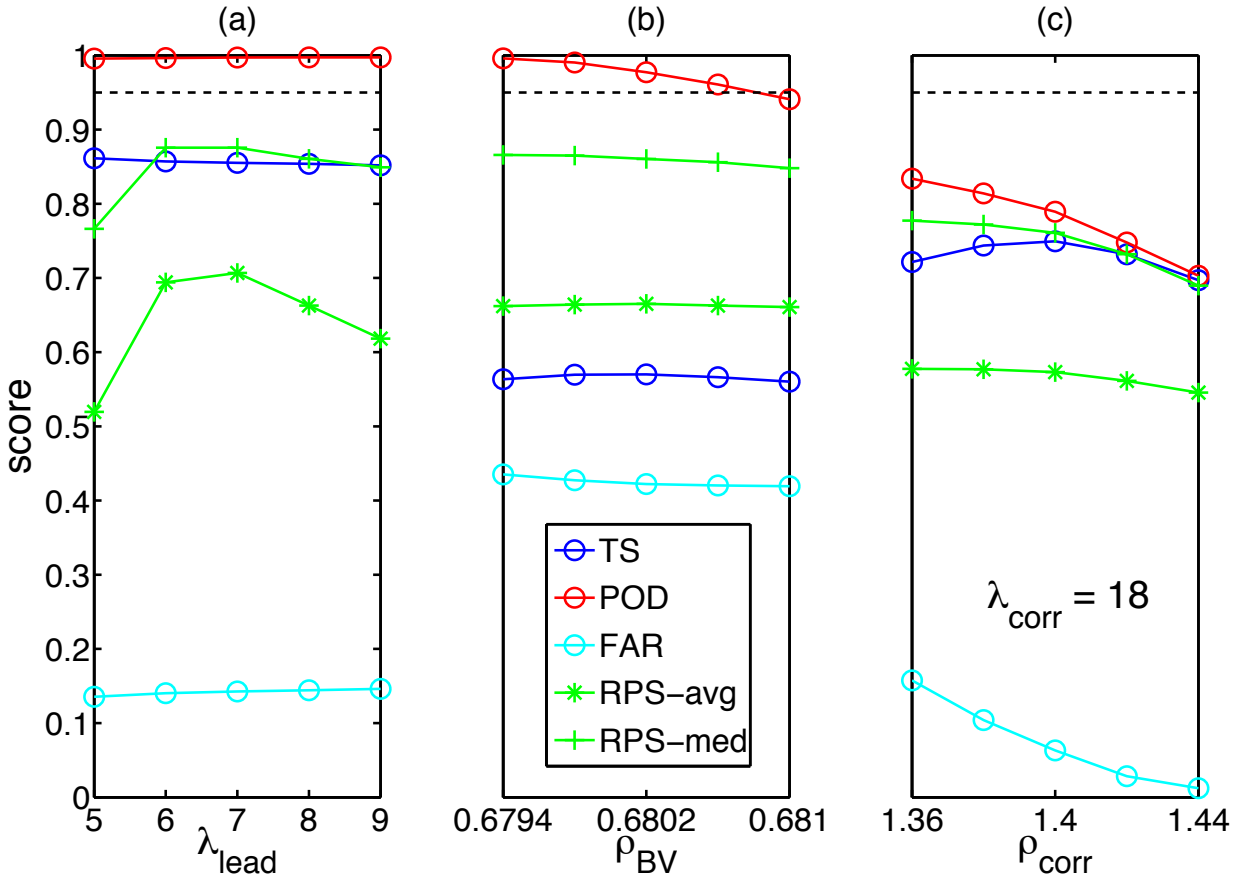

Figure S3-1. Tuning the flow reversal forecasts methods by varying (a) ρ_{corr} for the correlation test, (b) ρ_{BV} for the BV test, and (c) λ_{lead} for lead test. The dashed line is at 95%. There are tradeoffs among the various skill scores (POD, TS, RPS-avg, RPS-med) and costs (FAR). The chosen, final parameters $\lambda_{\text{lead}} = 7$, $\rho_{\text{BV}} = 0.6802$, and $\rho_{\text{corr}} = 1.4$ (with $\lambda_{\text{corr}} = 18$) appear in the middle of each plot.

APPENDIX S3: Flow reversal forecast tuning

In Fig. S3-1, we present skill score curves as the tuning parameters of the three flow reversal forecasts are varied. We used a sequence of plots of this type to inform our tuning of the various flow reversal tests.

In Fig. S3-2, we also present warning time histograms for the different tests. If early detection of flow reversals is desirable, then the warning times tell us how the tests compare.

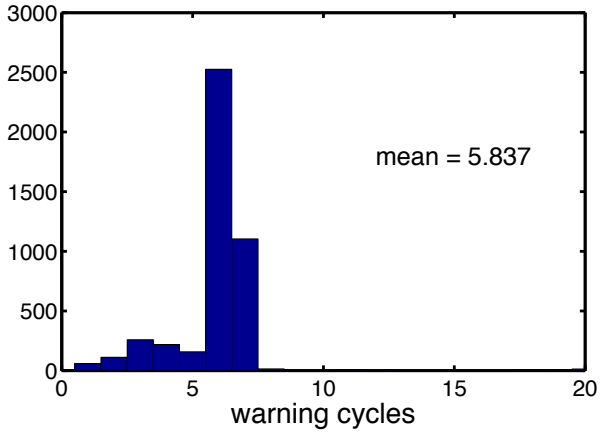

(a) lead

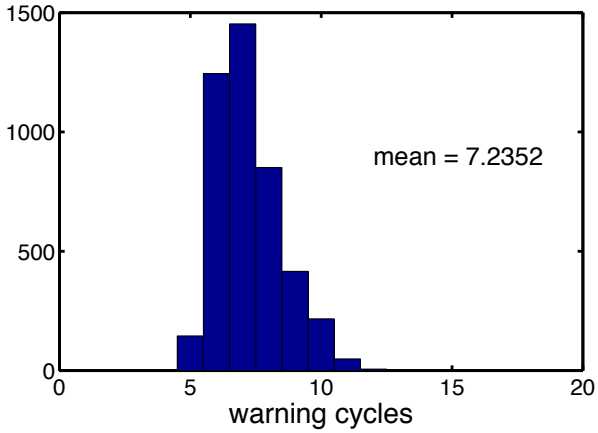

(b) bred vector

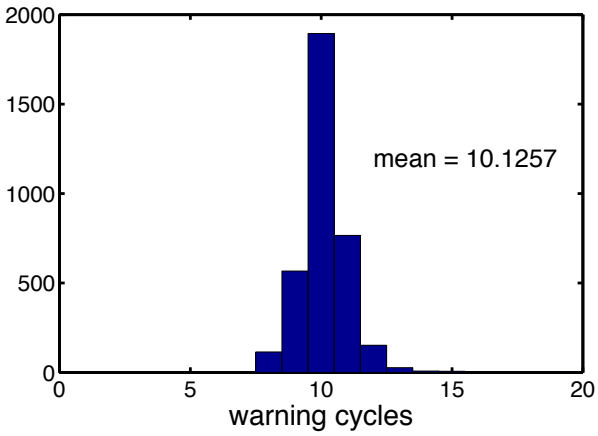

(c) correlation

Figure S3-2. Warning time distributions for the three flow reversal tests, in units of 30 s analysis cycles. The warning time is the time interval between the test being triggered and observation of the the actual flow reversal. The correlation test gives the earliest average warning time, followed by the BV and lead tests.

REFERENCES

Annan, J. D. and Hargreaves, J. C. 2004. Efficient parameter estimation for a highly chaotic system. *Tellus* **56A**, 520–526.

Baake, E., Baake, M., Bock, H. and Briggs, K. 1992. Fitting ordinary differential equations to chaotic data. *Physical Review A* **45**(8), 5524–5529.

Danforth, C. M. and Kalnay, E. 2008a. Impact of Online Empirical Model Correction on Nonlinear Error Growth. *Geophysical Research Letters* **35**, L24805.

Danforth, C. M. and Kalnay, E. 2008b. Using Singular Value Decomposition to Parameterize State-Dependent Model Errors. *Journal of the Atmospheric Sciences* **65**, 1467–1478.

Danforth, C. M., Kalnay, E. and Miyoshi, T. 2007. Estimating and Correcting Global Weather Model Error. *Monthly Weather Review* **135**, 281–299.

Ehrhard, P. and Müller, U. 1990. Dynamical behaviour of natural convection in a single-phase loop. *Journal of Fluid Mechanics* **217**, 487–518.

Evensen, G. 1994. Sequential data assimilation with a nonlinear quasi-geostrophic model using Monte Carlo methods to forecast error statistics. *Journal of Geophysical Research* **99**, 10143–10162.

Evensen, G. 2003. The Ensemble Kalman Filter: theoretical formulation and practical implementation. *Ocean Dynamics* **53**, 343.

Golub, G. H. and van Loan, C. F. 1996. *Matrix computations*. Johns Hopkins University Press, Baltimore, MD.

Gorman, M., Widmann, P. J. and Robbins, K. A. 1986. Nonlinear dynamics of a convection loop: a quantitative comparison of experiment with theory. *Physica D* **19**, 255–267.

Hunt, B. R., Kostelich, E. J. and Szunyogh, I. 2007. Efficient data assimilation for spatiotemporal chaos: A local ensemble transform Kalman filter. *Physica D* **230**, 112–126.

Kalnay, E. 2002. *Atmospheric Modeling, Data Assimilation and Predictability*. Cambridge University Press, Cambridge, UK.

Kalnay, E., Li, H., Miyoshi, T., Yang, S.-C. and Ballabrera-Poy, J. 2007. 4-D-Var or ensemble Kalman filter?. *Tellus* **59A**, 758–773.

Li, H., Kalnay, E., Miyoshi, T. and Danforth, C. M. 2009. Accounting for Model Errors in Ensemble Data Assimilation. *Monthly Weather Review* **137**(10), 3407–3419.

Matlab. 2009. The MathWorks, Inc. 3 Apple Hill Drive, Natick, MA 01760-2098 USA. Online at: `http://www.mathworks.com/`

Savely, R. T., Cockrell, B. F. and Pines, S. 1972. Apollo experience report – onboard navigational and alignment software, *Technical report*, NASA.

Welander, P. 1967. On the oscillatory instability of a differentially heated fluid loop. *Journal of Fluid Mechanics* **29**, 17–30.

Whitaker, J. S. and Hamill, T. M. 2002. Ensemble Data Assimilation without Perturbed Observations. *Monthly Weather Review* **130**, 1913–1924.

Yang, S.-C., Baker, D., Li, H., Cordes, K., Huff, M., Nagpal, G., Okereke, E., Villafañe, J., Kalnay, E. and Duane, G. S. 2006. Data Assimilation as Synchronization of Truth and Model. *Journal of the Atmospheric Sciences* **63**, 2340–2354.